ACS OMEGA

Open Access

http://pubs.acs.org/journal/acsodf

Article

Effects of Inherent Minerals on Pyrolysis Behavior and Kinetics of Jimsar Oil Shale

Ran Cao, Dong Yang, Zhiqin Kang, Dongwei Huang, Zhenni Cui, and Yang Lu*

Cite This: *ACS Omega* 2023, 8, 40396−40406

Read Online

ACCESS | Metrics & More | Article Recommendations

ABSTRACT: In order to reveal the influences of different inherent minerals on the pyrolysis behavior and kinetics of oil shale, decarburization, and desilication, samples were obtained by pickling and demineralization. The influence of inherent minerals on the activation energy of oil shale at different conversion rates and the pyrolysis kinetic model were researched by the equal conversion method and principal curve method. The results demonstrated that the average and maximum weight loss rates and volatile release characteristic index of JM-C were lower than that of JM-R; however, JM-S appeared with the opposite trend. At the initial stage (α = 0.2−0.6), the pyrolysis activation energy of JM-C was basically the same as that of JM-R, while the pyrolysis activation energy of JM-S decreased. At the later stage (α = 0.6−0.8), the pyrolysis activation energy of JM-C was higher than that of JM-R, while the activation energy of JM-S was between JM-C and JM-R. The existence of inherent carbonates reduced the pyrolysis activation energy of oil shale, but only at the later stage of pyrolysis. In addition, the existence of inherent carbonates changed the pyrolysis kinetic model of oil shale from an order model to a one-dimensional diffusion model, encompassing $f(\alpha) = (1 - \alpha)^{2.5}$ and $f(\alpha) = 0.5\alpha^{-1}$. However, the existence of inherent silicates increased the activation energy of oil shale pyrolysis. Moreover, its mechanism was consistent with the original model, namely, an order model, $f(\alpha) = 1 - \alpha$.

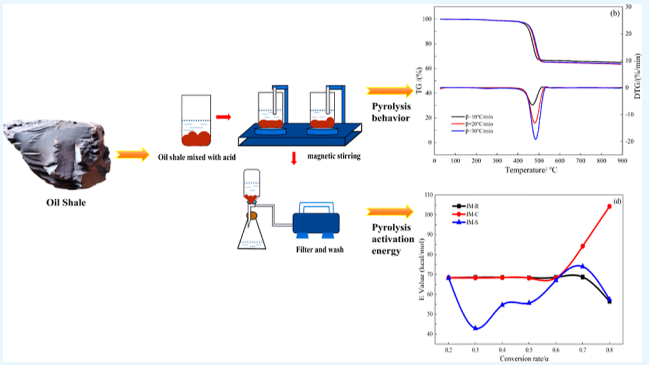

1. INTRODUCTION

China is abundant in oil shale resources,[1,2] with shale oil reserves ranking second worldwide.[3] These resources are widely distributed, mainly located in Xinjiang, Jilin, Liaoning, and Guangdong provinces.[4] Oil shale belongs to the class of sedimentary rock, characterized by its high organic matter content,[5,6] and the shale oil produced by its pyrolysis presents properties similar to those of natural oil. Consequently, it is a promising unconventional oil and gas energy source.[7,8] Oil shale organic matter consists mainly of kerogen and some soluble bitumen.[9] Kerogen is a polymeric substance with a reticulate structure[10] and serves as the primary source of pyrolytic oil and gas.[11,12] Oil shale has a rich inorganic skeletal structure,[13,14] and its inherent minerals mainly include clay minerals (such as kaolinite, montmorillonite, and illite), carbonate minerals (dolomite and calcite), quartz, and traces of pyrite.[15] The inherent minerals in oil shale exhibit uneven distribution and are closely cross-linked with organic matter.[16,17] In general, different inherent minerals impose various influences on the pyrolysis of oil shale, in which carbonates promote the pyrolysis of organic matter in oil shale, while silicates inhibit it.[18] Therefore, inherent minerals exert a remarkable influence on the pyrolysis behavior and mechanism of organic matter within oil shale.

Researchers worldwide have conducted comprehensive investigations into the behavior and kinetics of inherent minerals in oil shale pyrolysis. Through thermogravimetric analysis, Cai et al. observed an increase in the weight loss rate of Yaojie and Longkou oil shale following acid washing demineralization, and that the increase in porosity promoted the pyrolysis of oil shale.[19] Zhang et al. carried out thermogravimetric analysis and found that after acid washing demineralization of Longkou oil shale, carbonate rock could catalyze pyrolysis of organic matter, and silicates could inhibit the organic matter decomposition; the acid washing demineralization lowered the initial temperature in the process of oil shale pyrolysis, improving its efficiency.[20] By exploring how minerals impacted Jimsar oil shale pyrolysis and adopting the Friedman method for kinetic analysis, Pan et al. discovered that inherent minerals did not remarkably impact organic

Received: July 4, 2023
Accepted: September 22, 2023
Published: October 16, 2023

Table 1. Proximate Analysis and Ultimate Analysis of Jimsar Oil Shale

sample	proximate analysis/ω_{ad} %				ultimate analysis/ω_{ad} %				
	M	A	V	FC	C	H	O	N	S_t
JM-R	0.15	52.05	43.86	3.94	39.31	5.02	4.69	1.39	0.79

Table 2. Ash Composition Analysis of Jimsar Oil Shale

sample	ash composition/%								
	MgO	CaO	Al_2O_3	SiO_2	Fe_2O_3	SO_3	TiO_2	P_2O_5	others
JM-R	5.48	7.24	11.91	62.27	6.15	1.55	0.69	0.92	3.79

matter pyrolysis reaction in Jimsar oil shale and the original and demineralized oil shale appeared to have same activation energy distribution of pyrolysis.[21] Chang et al. removed minerals from Huadian and Balikun oil shales by using acid washing and performed kinetic analysis under the assistance of the Coats−Redfern method. As found, when the temperature changed from 350 to 510 °C, hydrochloric acid washing and hydrofluoric acid−hydrochloric acid pickling reduced and increased the apparent activation energy by approximately 10 and 30 kJ/mol, respectively.[22] Sert et al. divided the pyrolysis of a Turkish oil shale into two temperature ranges for kinetic analysis. It was showed that the activation energy elevated after HCl pickling in one reaction zone, the removal of silicates slightly decreased the activation energy, and the activation energy decreased in the second reaction zone due to the removal of inorganic minerals from the organic structure.[23]

In summary, the inherent carbonate and silicate minerals of oil shale crucially impacted the pyrolysis behavior of organic matter. However, studies have mainly focused on the way inherent minerals impact the properties and average activation energy exhibited by oil shale pyrolysis products. Therefore, we investigated the pyrolysis behavior exhibited by intact and demineralized oil shale samples using the thermal analysis method, studied how inherent minerals affected the kinetic mechanism of different pyrolysis stages of oil shale using the isoconversion method (including the FWO and KAS methods), and derived the mechanism function of pyrolysis at different samples using the master curve method. The aforementioned studies provide theoretical references for the catalytic conversion as well as the clean and efficient utilization of oil shale.

2. MATERIAL AND METHODS

2.1. Sample Preparation. The study object was Jimsar oil shale in Xinjiang. The samples were crushed and sieved to bring the particle size to less than 0.15 mm. Industrial and elemental analyses were performed following the Industrial Analysis Method of Coal (GB/T212-2008) and Elemental Analysis of Coal (GB/T31391-2015), respectively, and the results are summarized in Table 1. As observed, Jimsar oil shale was characterized with a high volatile content and a low ash content (Table 1). Moreover, the atomic ratio of H/C was 1.53 and that of O/C was 0.09. Therefore, according to the Van Krevelen diagram of the kerogen type, this kerogen belongs to type I,[24] with a high oil production potential.[25,26] The ash composition analysis of Jimsar oil shale using X-ray fluorescence revealed that the main components of inherent minerals of Jimsar oil shale encompassed silicon and aluminum, in addition to iron and some other elements (calcium and magnesium; Table 2).

2.2. Demineralization. Ten grams of the original sample of Jimsar oil shale (JM-R) was added to 160 mL of 6 mol/L HCl and 80 mL of 40 vol % HF, respectively, and stirred at 60 °C for 4 h using a magnetic mixer. Afterward, the demineralized samples were vacuum-filtered and washed until the pH was neutral. The acid-washed demineralized samples of hydrochloric acid (JM-C) and hydrofluoric acid (JM-S) were obtained. Finally, the samples received 24 h of drying treatment at 105 °C in an oven.

2.3. Experimental Equipment. A NETZSCH STA 449 F5 thermogravimetric analyzer served for investigating the pyrolysis behavior and the kinetics of the raw and demineralized oil shale samples. Samples were heated to 20−900 °C, and N_2 was continuously introduced at 40 mL/min, where the TG−DTG diagram in this experiment was calculated and plotted according to the dry and ash free base. The study also examined the effect of heating rates (10, 20, and 30 °C/min) on the pyrolysis characteristics.

2.4. Pyrolysis Characteristic Parameters. For a more in-depth examination of the pyrolytic properties and behavior exhibited by the three Jimsar oil shale samples, our study mainly paid attention to the five pyrolysis characteristic parameters

$$D = \frac{\left(\frac{dw}{dt}\right)_{max} \times \left(\frac{dw}{dt}\right)_{mean}}{T_V \times T_{max} \times \Delta T_{1/2}} \quad (1)$$

(1) Volatile initial temperature (T_v): the temperature when the volatiles of oil shale begin to be released, which is an important index to measure the difficulty of volatile release of oil shale. It refers to the point on the DTG curve when the weight loss rate is 1 wt % min^{-1}.

(2) T_{max}: the temperature corresponding to the maximum weight loss rate of the DTG curve.

(3) $\Delta T_{1/2}$: the half-peak width corresponding to the temperature interval $(d\omega/dt)/(d\omega/dt)_{max} = 1/2$, which indicates the concentration of the volatile fraction released from oil shale pyrolysis.[27,28]

(4) $(d\omega/dt)_{mean}$ and $(d\omega/dt)_{max}$ denote the average and maximum weight loss rates during oil shale pyrolysis, respectively.

(5) Integrated volatile release characteristic index (D), for measuring the release performance of volatiles and reflecting the pyrolytic reactivity of the oil shale.[29,30]

2.5. Kinetics Analysis. Kinetic analysis method helps to comprehensively explain the reaction mechanism during oil shale pyrolysis (JM-R, JM-C, and JM-S). Based on the multiple scan rate method and Arrhenius equation, the kinetic parameters were solved based on multiple TG curves at

https://doi.org/10.1021/acsomega.3c04780
ACS Omega 2023, 8, 40396−40406

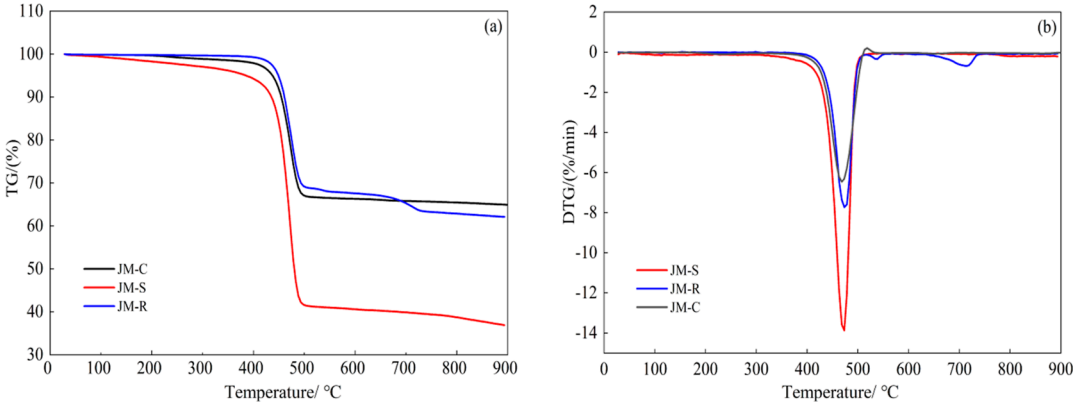

Figure 1. TG and DTG curves of pyrolysis of original and demineralized samples (a) TG; (b) DTG.

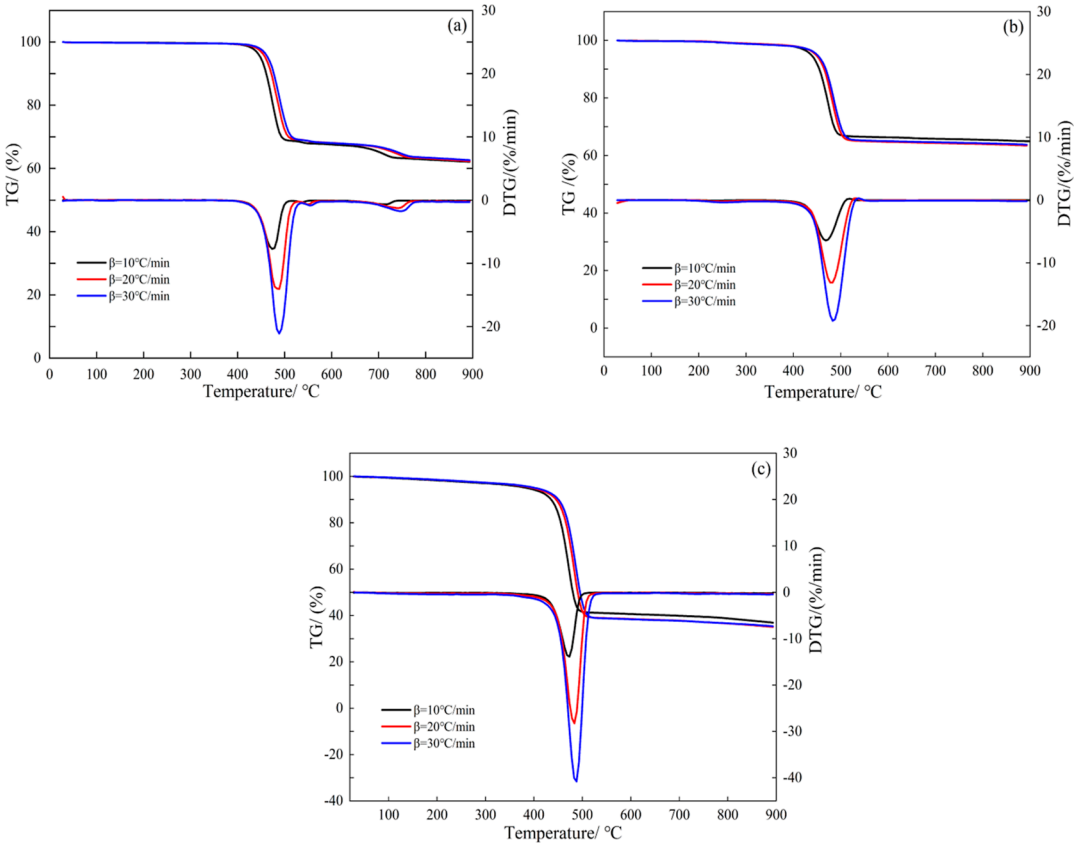

Figure 2. Heating rate-dependent TG and DTG curves of original and demineralized samples (a) JM-R; (b) JM-C; (c) JM-S.

various heating rates. The equations of the nonhomogeneous reaction system in the solid fuel process are as follows:[31,32]

$$\frac{d\alpha}{dt} = kf(\alpha) \text{ or } \frac{d\alpha}{dt} = \frac{A}{\beta}\exp\left(-\frac{E}{RT}\right) \quad (2)$$

In eq 2, t means the reaction time, $f(\alpha)$ denotes a reaction mechanism function, α is the conversion rate, $k(T)$ is the reaction rate constant related to the reaction temperature, A denotes the pre-exponential factor, β represents the heating rate, E denotes the reaction activation energy, and R is the gas constant [8.3145 J (mol K)$^{-1}$].

$$\alpha = \frac{m_o - m_t}{m_o - m_f} \quad (3)$$

In eq 3, m_o, m_t, and m_f denote the initial sample mass, the mass at the pyrolysis time t, and the final sample mass, respectively.

In this experiment, the FWO[33] and KAS methods[34] were employed to determine the kinetic parameters. The expression of the FWO method is as follows:

$$\ln\beta = \ln\left(\frac{AE}{RG(\alpha)}\right) - 5.331 - 1.0516\frac{E}{RT} \quad (4)$$

When conversion rate α is constant, a linear fit can be obtained for ln β and $1/T$. Then, the slope of the line can be figured out: 1.0516 E/R. Finally, the pyrolysis activation energy E can be gained.

The KAS method is expressed as follows:

https://doi.org/10.1021/acsomega.3c04780
ACS Omega 2023, 8, 40396−40406

Table 3. Heating Rate-Dependent Pyrolysis Characteristics of Oil Shale and Demineralized Samples

sample	heating rate (°C/min)	T_v (°C)	T_{max} (°C)	$(d\omega/dt)_{max}$ (% min)	$(d\omega/dt)_{mean}$ (% min)	$\Delta T_{1/2}$ (°C)	$D \times 10^{-7}$ (%^{2} min^{-2}°C^{-3})
JM-R	10	433.4	473.5	7.72	0.44	35.33	4.69
	20	432.6	488.6	14.03	0.86	38.02	14.98
	30	430.0	488.8	21.11	1.31	38.82	33.93
JM-C	10	428.2	468.2	6.45	0.40	44.22	3.02
	20	425.9	477.9	13.13	0.80	46.43	11.13
	30	420.9	482.9	19.36	1.27	47.91	25.15
JM-S	10	418.2	473.3	13.87	0.72	33.01	15.34
	20	403.3	483.3	28.26	1.49	33.25	65.12
	30	375.9	487.9	40.79	2.25	35.56	140.71

$$\ln\left(\frac{\beta}{T^2}\right) = \ln\left(\frac{AE}{RG(\alpha)}\right) - \frac{E}{RT} \quad (5)$$

In the presence of a linear fit for ln (β/T^2) and $1/T$, the slope of the line can then be obtained: E/R. Finally, the pyrolysis activation energy E can be figured out.

3. RESULTS AND DISCUSSION

3.1. Impact of Inherent Minerals on Oil Shale Pyrolysis Behavior. Figure 1 represents the TG−DTG curves for the raw and demineralized samples of Jimsar oil shale at 10 °C/min when the temperature changed from 20 to 900 °C. As the temperature increased, the oil shale decomposed because of the influence of heat, with physicochemical changes occurring in its macromolecular structure (Figure 2a). Among the different physiochemical changes, the weight loss behaviors exhibited by the original and demineralized samples differed. Within 600−800 °C, the pyrolytic weight loss of JM-R was larger than that of JM-C since the thermal decomposition of carbonate minerals facilitated kerogen[35] cracking and volatile release in this temperature range. However, the pyrolysis weight loss of JM-S was much larger than that of JM-R and JM-C, indicating the suppressive influence of silicate on thermal decomposition of organic kerogen in oil shale. As shown in Figure 2b, the three samples had obvious weight loss peaks from 350 to 550 °C, which were caused by the cracking of organic kerogen in oil shale. Chemical reactions (the depolymerization of macromolecules, C−C and C−H fracture, and so forth) were accompanied by the generation and release of many free radicals[36] and the liberation of volatile oil and gas. The order of the pyrolysis weight loss rate was JM-S > JM-R > JM-C. The removal of carbonate and silicate minerals affected the weight loss rate of pyrolysis, indicating that carbonate and silicate minerals promoted and inhibited the cracking of organic matter in oil shale, respectively. In the temperature range of 630−750 °C, JM-R presented a significant weight loss peak, owing to carbonate mineral decomposition, which conformed to the conclusions of Yan et al.[37]

3.2. Impact of Inherent Minerals on Oil Shale Pyrolysis Characteristics. Figure 2 displays the heating-rate-based TG and DTG curves for the original and demineralized samples and the pyrolysis characteristics. As can be seen from Table 3 that lists the results, when the heating rate was 10 °C/min, compared with JM-R, the volatile initial precipitation temperatures of JM-C and JM-S were reduced, which was attributed to the fact that pickling increased the size of the pores inside the oil shale, promoting the increase in the internal heat transfer rate.[38] As shown in Table 2, the initial analysis temperature of the pyrolysis volatilization was greatly reduced because of the removal of a large amount of silicate after pickling. The peak temperatures corresponding to the maximum weight loss rates of JM-C and JM-S were reduced, indicating that acid demineralization led to oil shale pyrolysis proceeding at a lower temperature. Relative to the original sample, JM-C had lower maximum and average weight loss rates, and JM-S achieved remarkably higher maximum and average weight loss rates, because the existence of carbonate and silicate minerals promoted and inhibited thermal decomposition of oil shale, respectively. Besides, at 10 °C/min heating rate, the full width at half-maximum loss rate of the temperature range of JM-C increased by 8.89 °C relative to that for JM-R. This was observed given that the removal of carbonate minerals widened the temperature range regarding oil shale pyrolysis, decreasing the pyrolysis volatile concentration, thus slowing down the pyrolysis rate. The full width at half-maximum loss rate of the temperature range of JM-S decreased by 2.32 °C relative to that for JM-R, because of the narrowed full width at half-maximum of oil shale pyrolysis that resulted from the removal of silicate minerals and the release of pyrolysis volatilization in a smaller temperature range, and the more concentrated the pyrolysis reaction, the faster the pyrolysis rate.

The initial analysis temperatures (T_v) of the pyrolysis volatilizing of JM-R, JM-C, and JM-S decreased as the heating rate increased because increased heating rate enlarged oil shale internal heat supply and accelerated the organic matter reaction speed. Besides, T_{max} gradually increased with the heating rate, owing to the "thermal hysteresis" phenomenon in the pyrolysis process. The difference between internal and external temperatures increased with the pyrolysis process, forming a temperature gradient, which led to the oil shale pyrolysis process moving to the zone with high temperature. When the heating rate increased, $(d\omega/dt)_{max}$ and $(d\omega/dt)_{mean}$ of the original and demineralized samples increased. This was because as heating rate increased, the heat transfer rate elevated, and the depolymerization of macromolecules was accelerated, thus resulting in the easier release of volatile products and precipitation of the pyrolysis oil and gas. The full width at half-maximum $\Delta T_{1/2}$ indicating the concentration degree of pyrolysis volatilization release increased as heating rate increased (Table 3), which was because the increase in heating rate led to insufficient heat absorption time of oil shale, making the reaction is not concentrated, and the reduced concentration degree of pyrolysis volatilization release reduces.

The composite volatile release characteristic index (D) essentially indicates the oil shale pyrolysis reactivity. Higher values of D indicate higher volatile release performance and better pyrolysis reactivity. D for JM-C at the three heating rates was lower relative to that for JM-R. At 10 °C/min, D for JM-C

https://doi.org/10.1021/acsomega.3c04780
ACS Omega 2023, 8, 40396−40406

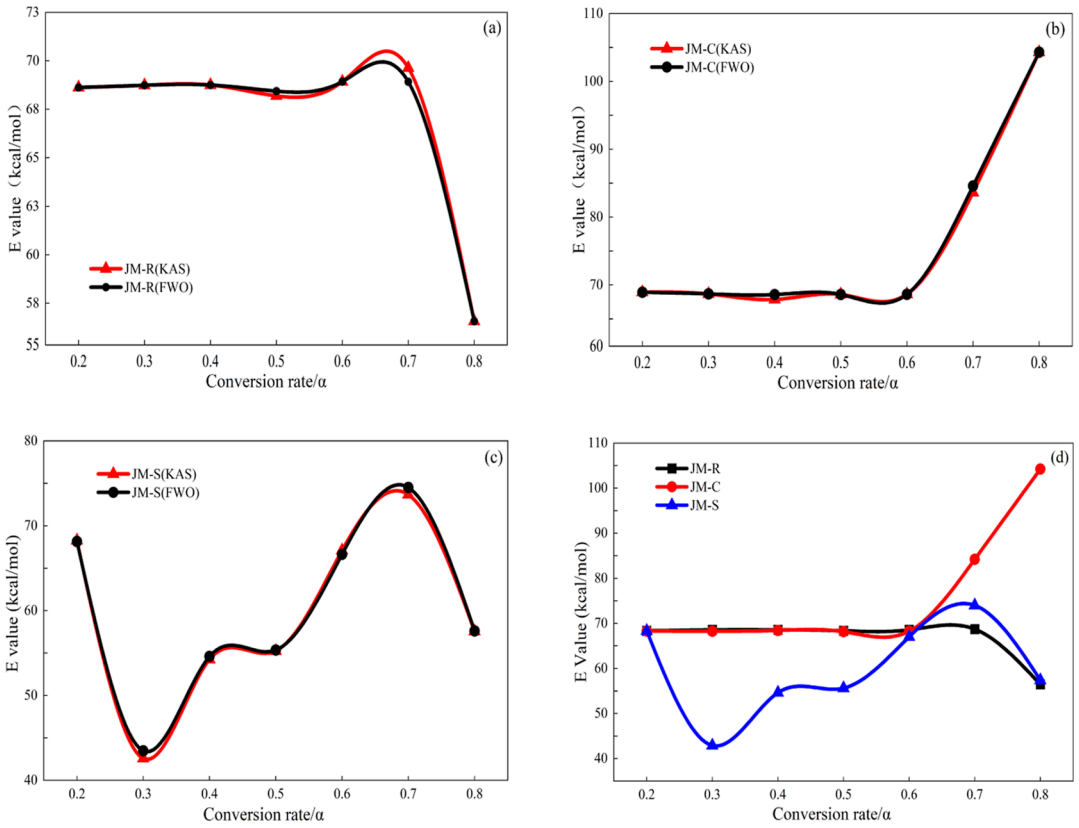

Figure 3. Pyrolysis activation energies at each conversion rate for different samples obtained using the KAS and FWO methods: (a) JM-R; (b) JM-C; (c) JM-S; (d) comparison of pyrolysis activation energies of samples from the KAS method.

was 36% lower than that of the original. As noted above, this implied that carbonate minerals promoted volatilization and remarkably enhanced oil shale pyrolysis reactivity. However, *D* for JM-S was higher than that for JM-R under the three heating rates. At 10 °C/min, the *D* for JM-S was 226% higher than the original value. As aforementioned, silicate minerals inhibited volatilization release and greatly reduced oil shale pyrolysis reactivity.

3.3. Impact of Inherent Minerals on Pyrolysis Kinetics. *3.3.1. Activation Energy from FWO and KAS Methods.* FWO and KAS methods were adopted to investigate the pyrolysis mechanism exhibited by the original and demineralized samples of the Jimsar oil shale.[39] The three kinetic factors of the sample pyrolysis reaction were calculated: activation energy (E), pre-exponential factor (A), and mechanism function $f(\alpha)$. According to eq 5, at the conversion rate (α) of 0.2−0.8, the pyrolysis activation energy curves of JM-R, JM-C, and JM-S are described in Figure 3.

The correlation coefficients (R^2) of E values of the three samples were larger than 0.98, indicating that the results were highly accurate. The variation trends of the E values calculated by the FWO and KAS methods were consistent under different conversion rates, and the E values calculated by the two methods revealed a small difference, suggesting that the calculation results were accurate and credible (Figure 3). It can be seen from Figure 3a, For the Jimsar oil shale, the pyrolysis activation energy was initially stable and then decreased rapidly with the conversion rate (Figure 3). At 0.2−0.6 conversion rate and 440−500 °C, the pyrolysis activation energy remained at 68−69 kcal/mol because −COOH, C−O−C, C═C, and other kerogenaceous functional groups of oil shale were broken and free radicals were formed in this temperature range. Various free radicals reacted with each other and combined into small molecular compounds, generating gaseous products, such as CO_2 and CO.[40] The volatiles of oil shale pyrolysis began to separate out rapidly, producing oil and gas. A series of chemical changes occurred, such as C−C and C−H fractures and condensation reactions. At 0.6−0.7 conversion rate, the corresponding temperature range was 530−570 °C. The pyrolysis activation energy slightly increased, which was due to volatilization of the pyrolysis oil and combination of the hydrogen and hydrogenated aromatic rings in the volatilized aliphatic hydrocarbons of pyrolysis fragments to form aromatic compounds,[41] increasing the activation energy required for pyrolysis.

At 0.7−0.8 conversion rate, the corresponding temperature range was 580−700 °C. The pyrolysis activation energy decreased rapidly because of the catalytic influence of its inherent carbonate minerals, which lowered the energy needed for pyrolysis reaction. As shown in Figure 3b, at α of 0.2−0.6, the pyrolysis activation energy of JM-C was similar to that of Figure 3a, and the change trend was consistent. At α of 0.6−0.8, the pyrolysis temperature corresponding to JM-C ranged from 580 to 680 °C, and the E value continued to rise at high temperature. The pyrolysis volatiles in the remaining samples were reduced; the proportions of ash and fixed carbon increased, and the pyrolysis reactivity decreased, thereby increasing the activation energy required for the pyrolysis reaction. Obviously, the increased conversion rate was accompanied by fluctuating pyrolysis activation energy of JM-S (Figure 3c). At 0.2−0.8 conversion rate, the corresponding temperature range was 450−550 °C. Compared with JM-R,

https://doi.org/10.1021/acsomega.3c04780
ACS Omega 2023, 8, 40396−40406

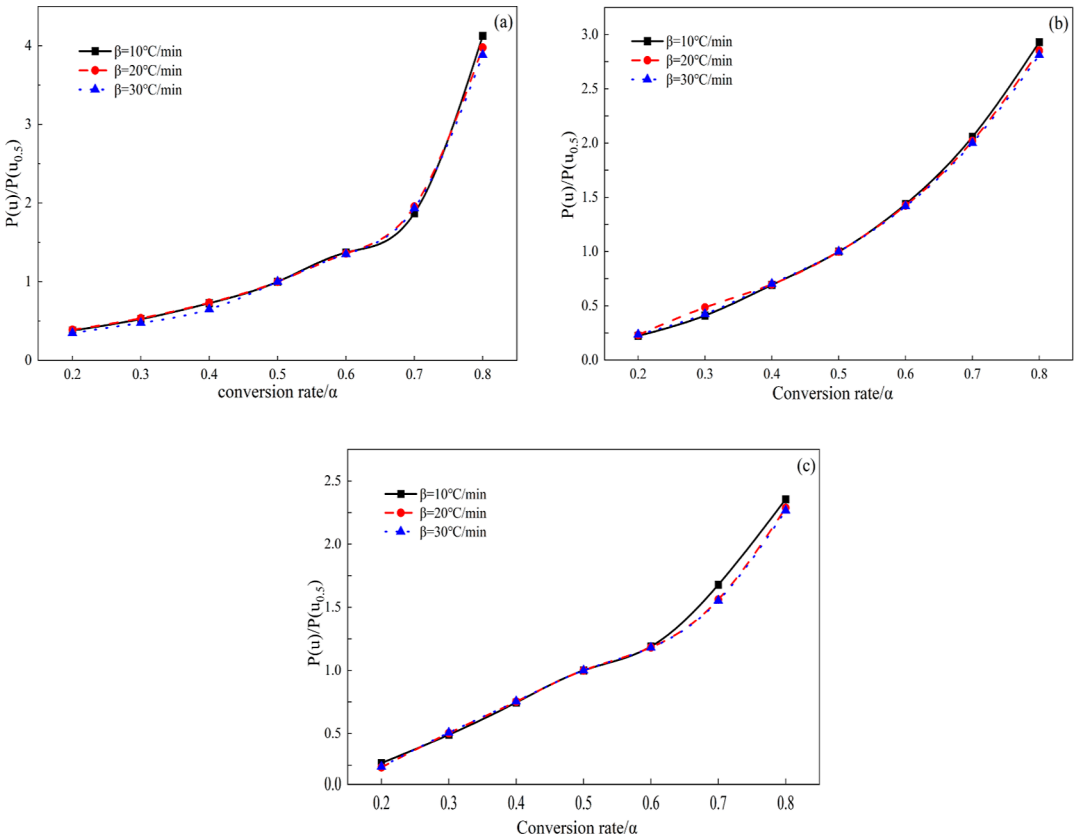

Figure 4. Heating rate-dependent experimental pyrolysis curves regarding oil shale and demineralized samples (a) JM-R; (b) JM-C; (c) JM-S.

JM-S had lower pyrolysis activation energy, because removing silicate minerals promoted oil shale organic matter pyrolysis. Thus, the activation energy required for the pyrolysis reaction fell.

Figure 3d displays the conversion rate-dependent change of pyrolysis activation energy based on the KAS method. At 0.2−0.6, the pyrolysis activation energy of JM-R and JM-C was basically similar, and at 0.6−0.8, the pyrolysis activation energy of JM-C was higher than that of JM-R. This was because the inherent carbonate minerals exerted a catalytic effect on oil shale pyrolysis, which contributed to enhancing pyrolysis of organic matter of oil shale, releasing more pyrolysis oil and pyrolysis gas, improving oil shale pyrolysis reactivity, and reducing the activation energy required for the pyrolysis reaction. At 0.2−0.6 conversion rate, the pyrolysis activation energy of JM-S was lower than that of JM-R, because the inherent silicate minerals suppressed pyrolysis of organic matter. Hydrofluoric acid pickling led to the removal of silicate minerals, and larger internal pores, which promoted mass and heat transfer influence as well as occurrence of the pyrolysis reaction and release of volatiles over a smaller temperature range. At 0.6−0.8 conversion rate, the activation energy of JM-S was between JM-C and JM-R, and the activation energy for JM-S was much closer to that for JM-R.

As observed, the average pyrolysis activation energy of JM-C was 75.91 kcal/mol, and that of JM-R was 67.06 kcal/mol, which was 8.85 kcal/mol lower than that of JM-C (Figure 3). It can be concluded that the existence of inherent carbonate minerals promoted organic matter pyrolysis and the volatile component release of oil shale. The energy required for the pyrolysis reaction decreased. The average pyrolysis activation energy of JM-S was 59.63 kcal/mol, which was 7.43 kcal/mol lower than that of JM-R. It can be seen that the existence of silicate minerals inhibited the kerogen organic matter cracking and increased the energy required for pyrolysis reaction, which was different from Pan,[21] who also studied the influence of inherent minerals on the pyrolysis behavior and kinetics of Jimsar oil shale, and pointed out that inherent minerals had no influence on the pyrolysis activation energy of Jimsar oil shale, owing to different compositions of the oil shale used. The contents of Na, Ca, and Fe in the oil shales used in this experiment were higher than those used by Pan et al. Since they existed in the form of carbonate, the catalytic influence on the pyrolysis reaction was better than that of the oil shale used by Pan et al. Overall, carbonate and silicate minerals promoted and inhibited the volatilization of organic matter in oil shale, respectively.

3.3.2. Most Possible Pyrolysis Kinetic Model Established by Principal Curve Method. Principal curve method is an analytical method used for establishing the most probable kinetic model (mechanism function) of the oil shale pyrolysis reaction.[42,43] It is more accurate than the traditional numerical decision-mechanism function analysis method. In eq 6, $G(\alpha)$ denotes the integral-form mechanism function, and T_0 is the reaction initial reaction temperature. The Jimsar oil shale revealed a slow pyrolysis speed at the initial reaction temperature (T_0). Thus, the lower limit of the integral on the right side of the kinetic eq 6 can be approximated by zero and be transformed into eqs 7 and 8

$$G(\alpha) = \int_0^\alpha \frac{1}{f(\alpha)}\,\mathrm{d}\alpha = \frac{A}{\beta}\int_{T_0}^{T} \exp\left(\frac{E}{RT}\right)\mathrm{d}T \quad (6)$$

https://doi.org/10.1021/acsomega.3c04780
ACS Omega 2023, 8, 40396−40406

Table 4. Common Reaction Mechanisms of Solid State Process

reaction mechanism	symbol	$f(\alpha)$	$G(\alpha)$
		order of reaction	
first-order	F_1	$1-\alpha$	$-\ln(1-\alpha)$
second-order	F_2	$(1-\alpha)^2$	$(1-\alpha)^{-1}-1$
third-order	F_3	$(1-\alpha)^3$	$[(1-\alpha)^{-2}-1]/2$
		diffusion	
one-way transport	D_1	$0.5\alpha^{-1}$	α^2
two-way transport	D_2	$[-\ln(1-\alpha)]^{-1}$	$(1-\alpha)\ln(1-\alpha)+\alpha$
three-way transport	D_3	$1.5(1-\alpha)^{2/3}[1-(1-\alpha)^{1/3}]^{-1}$	$[1-(1-\alpha)^{1/3}]^2$
Ginstling−Brounshtein equation	D_4	$1.5[(1-\alpha)^{-1/3}-1]^{-1}$	$(1-2\alpha/3)-(1-\alpha)^{2/3}$
		limiting surface reaction between both phases	
one dimension	R_1	1	α
two dimensions	R_2	$2(1-\alpha)^{1/2}$	$1-(1-\alpha)^{1/2}$
three dimensions	R_3	$3(1-\alpha)^{2/3}$	$1-(1-\alpha)^{1/3}$
		random nucleation and nuclei growth	
two-dimensional	A_2	$2(1-\alpha)[-\ln(1-\alpha)]^{1/2}$	$[-\ln(1-\alpha)]^{1/2}$
three-dimensional	A_3	$3(1-\alpha)[-\ln(1-\alpha)]^{2/3}$	$[-\ln(1-\alpha)]^{1/3}$
		exponential nucleation	
power law, $n = 1/2$	P_2	$2\alpha^{1/2}$	$\alpha^{1/2}$
power law, $n = 1/3$	P_3	$3\alpha^{2/3}$	$\alpha^{1/3}$
power law, $n = 1/4$	P_4	$4\alpha^{3/4}$	$\alpha^{1/4}$

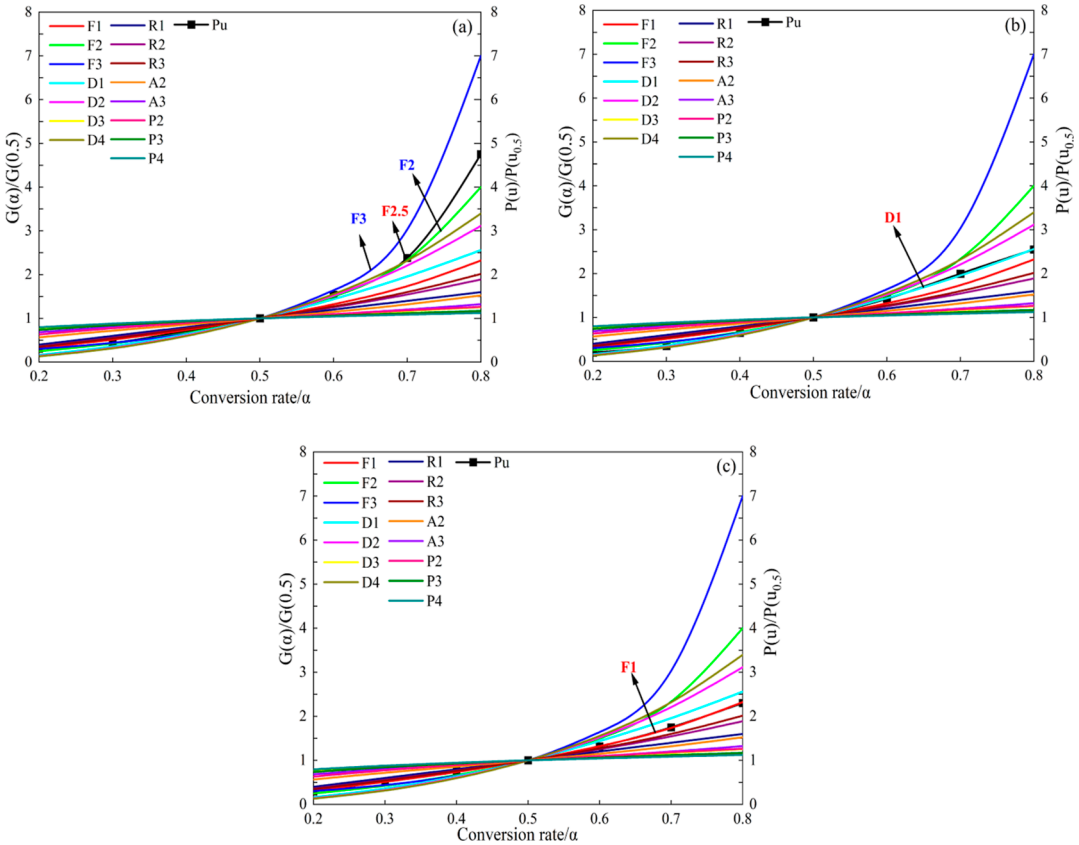

Figure 5. Comparison between experimental and standard pyrolysis curve comparison of different oil shale samples: (a) JM-R; (b) JM-C; (c) JM-S.

$$G(\alpha)=\int_0^\alpha \frac{1}{f(\alpha)}\,\mathrm{d}\alpha=\frac{A}{\beta}\int_{T_0}^{T}\exp\left(\frac{E}{RT}\right)\mathrm{d}T \tag{7}$$

$$\approx\frac{A}{\beta}\int_0^T \exp\left(\frac{E}{RT}\right)\mathrm{d}T=\frac{AE}{\beta R}P(u) \tag{8}$$

$$p(u)=\int_\infty^\alpha \frac{-\mathrm{e}^{-u}}{u^2}\,\mathrm{d}u \tag{9}$$

In above equations, $u = E/(RT)$ and $P(u)$ is the temperature integral.

Equation 9 is an expansion of $p(u)$, which shows that $p(u)$ is not differentiable around α and ∞. Therefore, $p(u)$ has no analytical solution and can be expressed as an approximation.

https://doi.org/10.1021/acsomega.3c04780
ACS Omega 2023, 8, 40396−40406

Doyle's rational approximation gives a sufficiently accurate result.[44]

$$P(u) = 0.00484 \cdot \exp(-1.051 - 6u) \quad (10)$$

We first used the equal conversion rate obtained from the above method for calculating the samples' pyrolysis activation energy. Then, we compared their experimental and the standard curve shapes to calculate the most possible mechanism function.

We selected $\alpha = 0.5$ as a reference point and substituted it into approximate eq 10 for acquiring eq 11. The ratio in eq 12 was obtained by dividing eq 10 by eq 11.

$$G(0.5) = \frac{AE}{\beta R} P(u_{0.5}) \quad (11)$$

$$\frac{G(\alpha)}{G(0.5)} = \frac{P(u)}{P(u_{0.5})} \quad (12)$$

The activation energies at different pyrolysis stages and the Doyle approximation formula described in eq 9 were calculated according to the equal conversion rates method of FWO and KAS, and experimental curves $P(u)/P(u_{0.5})$ at various heating rates were obtained. The average activation energies obtained by the equal conversion rate methods were calculated (Figure 4). The experimental curves of the original and demineralized samples of Jimsar oil shale at 10, 20, and 30 °C/min coincided, indicating that a single kinetic mechanism was adopted for the weight loss of this pyrolysis process. For the commonly used 15 kinetic model functions (Table 4),[45,46] we linearly fit α by $G(\alpha)/G(0.5)$ to acquire the standard curves (principal curves). The parameter u was then calculated based on the average activation energy and the corresponding temperature T in various pyrolysis stages. A series of experimental curves were obtained by the further linear fitting of α with $P(u)/P(u_{0.5})$(Figure 4). During the entire pyrolysis reaction stage, if coincident experimental curves were attained at various heating rates, it was used to describe the thermal weight loss process within such a temperature range using a single kinetic mechanism model. Furthermore, both experimental and standard curve shapes were compared. In the case of the experimental curve coincident with a standard curve, the reaction mechanism function was the kinetic model function that corresponded to the coincident standard curve. If the experimental curve and a certain standard curve did not overlap perfectly but the trend of change was consistent, it was impossible to confirm the most possible mechanism function by integer n.

Finally, the integral form of the kinetic mechanism function was substituted into eq 11. At a certain heating rate, different n values were taken at the interval of 0.1. Under the assistance of the least-squares method, a straight line was obtained by linear fitting of $EP(u)/(\beta R)$ with $G(\alpha)$. The line had a correlation coefficient (R^2) approaching 1, and the slope was pre-exponential factor A.

Subsequently, the experimental (20 °C/min) and the standard curves drawn using 15 kinetic model functions were compared; the shapes of the $P(u)/P(u_{0.5})$ and $G(\alpha)/G(0.5)$ curves were compared (Figure 5). In the case of the overlapping of the experimental curve with the standard curve, the mechanism function was the most possible mechanism function regarding the pyrolysis reaction. The experimental curve of the JM-R sample did not overlap with any standard curve but tended to be consistent with F_2 and F_3 and lied between them (Figure 5a), indicating that the kinetic mechanism could not be analyzed by integer n. The experimental curve of the JM-R sample did not overlap with any standard curve (Figure 5b or 5c). The experimental curves of JM-C and JM-S and the standard curves D_1 and F_1 appeared the same shape and almost overlapped, indicating that it was allowed to explain the thermal weight loss of their pyrolysis process could be explained using a single kinetic mechanism. Therefore, the thermal decomposition processes of JM-R and JM-S were order models, and the kinetic mechanism of JM-R was not consistent with the ideal model. In this regard, the value of n needed to be determined. However, the pyrolysis process of JM-C was a one-dimensional diffusion model.

As shown in Figure 5b, according to the comparison of the shape position of the experimental and the standard curves, the n value of the most probable mechanism function of JM-R was between 2 and 3. Next, using the formula of the order model in the kinetic mechanism function, the conversion rate α was substituted into $G(\alpha)$. According to eq 6, the average pyrolysis activation energy E and the corresponding temperature T at different pyrolysis stages were substituted into eq 9 to obtain $P(u)$. $EP(u)/(\beta R)$ was plotted as $G(\alpha)$. The slope is the line that refers to front pre-exponential factor A. An interval of 0.1 was adopted for confirming the optimal value of n for original oil shale samples (JM-R), and it was determined when the correlation coefficient R^2 of the fitted line was close to 1. The kinetic factors of the pyrolysis process of JM-R were determined. The results are shown in Table 5. The mechanism

Table 5. Kinetic Factors of Original and Demineralized Oil Shale Samples at Various Heating Rates

sample	β K min^{-1}	E kcal mol^{-1}	A s^{-1}	$f(\alpha)$	R^2
JM-R	10	67.06	2.051×10^{19}	$(1-\alpha)^{2.5}$	0.99931
	20		4.101×10^{19}		0.99931
	30		6.153×10^{19}		0.99931
JM-C	10	75.91	2.674×10^{21}	$0.5\alpha^{-1}$	0.98862
	20		1.622×10^{21}		0.98948
	30		2.298×10^{21}		0.98643
JM-S	10	59.63	2.286×10^{17}	$1-\alpha$	0.99842
	20		2.361×10^{17}		0.99744
	30		2.764×10^{17}		0.99838

function of the pyrolysis process of JM-R was $f(\alpha) = (1-\alpha)^{2.5}$, with its pre-exponential factors including 2.051×10^{19}, 4.101×10^{19}, and 6.153×10^{19}. The linear fitting correlation coefficients R^2 of the three samples of greater than 0.99 indicated that the calculation results of the three kinetic factors were credible.

The removal of silicates did not change the pyrolysis kinetic model of oil shale. JM-R and JM-S were order models whose corresponding mechanism functions were $f(\alpha) = (1-\alpha)^{2.5}$ and $f(\alpha) = 1-\alpha$. The diffusion speed of the oil shale samples through the product layer was much higher than the chemical reaction speed on the contact surface. Therefore, the chemical reaction rate decided the rates of the JM-R and JM-S pyrolysis processes. Removing carbonates changed the pyrolysis kinetic model regarding oil shale. JM-C was a 1D diffusion model whose mechanism function was $f(\alpha) = 0.5\alpha^{-1}$. Under this model, the diffusion speed was very slow and played a controlling role in the slowest step in the solid-phase reaction.

https://doi.org/10.1021/acsomega.3c04780
ACS Omega 2023, 8, 40396−40406

The chemical reaction speed was much greater than the diffusion speed; suggesting that the process was controlled by diffusion.

4. CONCLUSIONS

(1) The existence of carbonates promoted oil shale pyrolysis and volatile component release, whereas silicates inhibited thermal decomposition of organic kerogen. The pyrolysis weight loss of JM-C was less than that of JM-R from 600 to 800 °C, but the pyrolysis weight loss of JM-S was much greater than that of JM-R during the pyrolysis process. The order of the pyrolysis weight loss rates of the three samples was JM-S > JM-R > JM-C. The pyrolysis temperature intervals of JM-C and JM-C were higher than that of JM-R, and the degree of volatilization of pyrolysis decreased. The pyrolysis temperature interval of JM-S was lower than that of JM-R, and the pyrolysis reaction was more concentrated.

(2) At 10 °C/min heating rate, compared with JM-R, the initial analysis temperatures of JM-C and JM-S reduced by 5.2 and 15.2 °C, respectively. Relative to JM-R, JM-C had lower $(d\omega/dt)_{mean}$ and $(d\omega/dt)_{max}$, and JM-S had remarkably larger $(d\omega/dt)_{mean}$ and $(d\omega/dt)_{max}$. The index (D) of JM-C volatilized was 36% lower than that of the original sample, and the D value of JM-S was 226% higher than that of the original sample. Therefore, with increased heating rate increases the D value of the oil shale, and carbonate minerals and silicate minerals effectively improved and reduced the oil shale pyrolysis reactivity, respectively.

(3) At 0.2−0.6 conversion rate, JM-C and JM-R presented same pyrolysis activation energy, whereas the pyrolysis activation energy of JM-S decreased, indicating that the inherent silicate minerals played an inhibitory role in the cracking of oil shale kerogen. At 0.6−0.8 conversion rate, the pyrolysis activation energies of JM-C and JM-S were higher than that of JM-R. Hence, inherent carbonate minerals could catalyze oil shale pyrolysis and reduce its pyrolysis activation energy. Relative to JM-R, the average pyrolysis activation energy of JM-C was 8.85 kcal/mol higher, and that of JM-S was 7.43 kcal/mol lower.

(4) The existence of silicates did not change the pyrolysis kinetic model of oil shale. The thermal weight loss in the JM-R and JM-S pyrolysis processes could be, thus, interpreted using a single kinetic mechanism, which was an order model. The chemical reaction speed decided the pyrolysis speed, and the mechanism functions were $f(\alpha) = (1 - \alpha)^{2.5}$ and $f(\alpha) = 1 - \alpha$, respectively. The removal of carbonate changed the oil shale pyrolysis kinetic model of oil shale. JM-C was a 1D diffusion model in which the pyrolysis process was controlled by diffusion, and its mechanism function was $fs(\alpha) = 0.5\alpha^{-1}$.

AUTHOR INFORMATION

Corresponding Author

Yang Lu − *Key Lab of In-situ Property-improving Mining of Ministry of Education, Taiyuan University of Technology, Taiyuan 030024, P. R. China; The In-situ Steam Injection Branch of State Center for Research and Development of Oil Shale Exploitation, Taiyuan University of Technology, Taiyuan 030024, P. R. China;* orcid.org/0000-0003-2804-7073; Phone: +86-15535115452; Email: luyang0116@link.tyut.edu.cn

Authors

Ran Cao − *Key Lab of In-situ Property-improving Mining of Ministry of Education, Taiyuan University of Technology, Taiyuan 030024, P. R. China; The In-situ Steam Injection Branch of State Center for Research and Development of Oil Shale Exploitation, Taiyuan University of Technology, Taiyuan 030024, P. R. China*

Dong Yang − *Key Lab of In-situ Property-improving Mining of Ministry of Education, Taiyuan University of Technology, Taiyuan 030024, P. R. China; The In-situ Steam Injection Branch of State Center for Research and Development of Oil Shale Exploitation, Taiyuan University of Technology, Taiyuan 030024, P. R. China;* orcid.org/0000-0001-9730-6126

Zhiqin Kang − *Key Lab of In-situ Property-improving Mining of Ministry of Education, Taiyuan University of Technology, Taiyuan 030024, P. R. China; The In-situ Steam Injection Branch of State Center for Research and Development of Oil Shale Exploitation, Taiyuan University of Technology, Taiyuan 030024, P. R. China*

Dongwei Huang − *Key Lab of In-situ Property-improving Mining of Ministry of Education, Taiyuan University of Technology, Taiyuan 030024, P. R. China; The In-situ Steam Injection Branch of State Center for Research and Development of Oil Shale Exploitation, Taiyuan University of Technology, Taiyuan 030024, P. R. China*

Zhenni Cui − *State Key Laboratory of Clean and Efficient Coal Utilization, Taiyuan University of Technology, Shanxi 030024, China*

Complete contact information is available at: https://pubs.acs.org/10.1021/acsomega.3c04780

Notes

The authors declare no competing financial interest.

ACKNOWLEDGMENTS

The authors thank the financial support from the National Key Research and Development Program of China (no. 2019YFA0705501), China National Postdoctoral Program for Innovative Talents (no. BX2021209), and Fundamental Research Program of Shanxi Province (no. 202203021222089).

REFERENCES

(1) Yang, Q.; Guo, M.; Guo, W. Effects of associated minerals on the co-current oxidizing pyrolysis of oil shale in a low-temperature stage. *ACS Omega* **2021**, *6* (37), 23988−23997.

(2) Lu, Y.; Wang, Z.; Kang, Z.; Li, W.; Yang, D.; Zhao, Y. Comparative study on the pyrolysis behavior and Pyrolysate characteristics of Fushun oil shale during anhydrous pyrolysis and sub/supercritical water pyrolysis. *RSC Adv.* **2022**, *12* (26), 16329−16341.

(3) Wang, C.; Lu, Y.; Du, X.; Liu, Z. Characteristics and geophysical prediction of lithology heterogeneity of oil shale:Taking the 2nd Member of Funing Formation of Qintong sag, Subei Basin, as an example. *Oil Gas Geol.* **2015**, *36* (05), 814−821.

(4) Chen, L.; Jiang, Q.; Zhao, R.; Tang, F.; Zheng, A.; Song, S. Research on development potentiality of China's oil shale resources. *Mod. Chem. Ind.* **2009**, *29* (S1), 40−45.

(5) Lu, Y.; Wang, Y.; Xu, Y.; Li, Y.; Hao, W.; Zhang, Y. Investigation of ash fusion characteristics and migration of sodium during co-

combustion of Zhundong coal and oil shale. *Appl. Therm. Eng.* **2017**, *121*, 224−233.
(6) Liu, R.; Liu, Z.; Sun, P.; Xu, Y.; Liu, D.; Yang, X.; Zhang, C. Geochemistry of the Eocene Jijuntun Formation oil shale in the Fushun Basin, northeast China: Implications for source-area weathering, provenance and tectonic setting. *Geochemistry (Munich, Ger.)* **2015**, *75* (1), 105−116.
(7) Chen, Y.; Zhu, Z.; Zhang, L. Control actions of sedimentary environments and sedimentation rates on lacustrine oil shale distribution, an example of the oil shale in the Upper Triassic Yanchang Formation, southeastern Ordos Basin (NW China). *Mar. Pet. Geol.* **2019**, *102*, 508−520.
(8) Jia, H.; Sheng, J. J. Simulation study of huff-n-puff air injection for enhanced oil recovery in shale oil reservoirs. *Petroleum* **2018**, *4* (1), 7−14.
(9) Song, R.; Meng, X.; Yu, C.; Bian, J.; Su, J. Oil shale in-situ upgrading with natural clay-based catalysts: Enhancement of oil yield and quality. *Fuel* **2022**, *314*, 123076.
(10) Kang, Z.; Zhao, Y.; Yang, D. Review of oil shale in-situ conversion technology. *Appl. Energy* **2020**, *269*, 115121.
(11) Liu, H.; Liu, D.; Fang, C.; Xue, H.; Wang, H. Microwave heating technology of in-situ oil shale developing. *Acta Pet. Sin.* **2010**, *31* (04), 623−625.
(12) Taheri-Shakib, J.; Kantzas, A. A comprehensive review of microwave application on the oil shale: Prospects for shale oil production. *Fuel* **2021**, *305*, 121519.
(13) Bai, J.; Pan, S.; Wang, Q.; Chi, M.; Li, T. Pyrolysis characteristics of Inner Mongolia oil shales with different organic matter contents. *Chem. Ind. Eng. Prog.* **2017**, *36* (07), 2428−2435.
(14) Song, Y.; Liu, Z.; Sun, P.; Meng, Q.; Liu, R. A comparative geochemistry study of several oil shale-bearing intervals in the Paleogene Huadian Formation, Huadian Basin, Northeast China. *J. Earth Sci. China* **2017**, *28* (4), 645−655.
(15) Tong, B.; Yang, T.; Li, B.; Zhai, Y. Effect of internal minerals on supercritical liquefaction of oil shale. *Clean Coal Technol.* **2022**, *28* (06), 103−109.
(16) Lu, Z.; Lv, T.; Liu, L.; Liu, G. Experimental study on separation of oil shale and semi - coke by fluidization principle. *Oil Shale* **2019**, *36* (4), 449−461.
(17) Hakimi, M.; Abdullah, W.; Alqudah, M.; Makeen, Y. M.; Mustapha, K. A. Organic geochemical and petrographic characteristics of the oil shales in the Lajjun area, Central Jordan: Origin of organic matter input and preservation conditions. *Fuel* **2016**, *181*, 34−45.
(18) Chang, Z.; Chu, M.; Zhang, C.; Bai, S.; Lin, H.; Ma, L. Influence of inherent carbonates and silicates on pyrolytic products of Tailao oil shale. *CIESC J.* **2017**, *68* (04), 1582−1589.
(19) Cai, G.; Ma, M.; Xiong, Y.; Zhang, C.; Guo, W. Influence factors of acid treatment de-ashing of oil shales from Yaojie and Longkou. *Chem. Ind. Eng. Prog.* **2014**, *33* (01), 70−74.
(20) Zhang, Z.; Zhao, L.; Zhuang, L.; Li, Y.; Zhang, H. The effect of acid treatment on pyrolysis of Longkou oil shale. *Energy Sources, Part A* **2019**, *41* (13), 1605−1614.
(21) Pan, L.; Dai, F.; Huang, J.; Liu, S.; Li, G. Study of the effect of mineral matters on the thermal decomposition of Jimsar oil shale using TG-MS. *Thermochim. Acta* **2016**, *627*−*629*, 31−38.
(22) Chang, Z.; Chu, M.; Zhang, C.; Bai, S.; Lin, H.; Ma, L. Effect of demineralization on pyrolysis characteristics and kinetics of two Chinese oil shales. *J. Min. Sci.Techno* **2018**, *3* (3), 290−298. (in Chinese)
(23) Sert, M.; Ballice, L.; Yuksel, M.; Sağlam, M. The Effects of acid treatment on the pyrolysis of Goynuk oil shale (Turkey) by thermogravimetric analysis. *Oil Shale* **2012**, *29* (1), 51.
(24) Shen, J.; Yang, J.; Zhou, F.; Zhang, J.; Yang, G.; Qiu, Y.; Sun, Y. Study of kerogen type index through the calculation of organic elements. *J. Northeast Pet.* **2013**, *37* (05), 24−31.
(25) Xu, X.; Zhang, Y.; Huang, Y.; Xiong, X.; Li, X. Major controlling factors for development of oil shale in Liushagang Formation of Wushi sag, Beibuwan Basin. *Acta Pet. Sin.* **2013**, *34* (S2), 66−73.
(26) Gao, B.; Wu, X.; Zhang, Y.; Zhang, Y.; Chen, X.; Bian, R.; Li, Q. Hydrocarbon generation and evolution characteristics of older Zhangjiatan oil shale in southern Ordos Basin. *Pet. Geol. Exp.* **2022**, *44* (01), 24−32.
(27) Chen, J.; Wang, Y.; Lang, X.; Ren, X.; Fan, S. Evaluation of agricultural residues pyrolysis under non-isothermal conditions: Thermal behaviors, kinetics, and thermodynamics. *Bioresour. Technol.* **2017**, *241*, 340−348.
(28) Ma, M.; Li, L.; Gao, S. Research progress on coal maceral pyrolysis characteristics. *Coal Chem. Ind.* **2022**, *50* (03), 86−89.
(29) Wei, L.; Li, R.; Li, A.; Li, Y.; Jiang, X. Thermogravimetric Analysis on the Pyrolysis Characteristics of Pulverized Coal. *Proc. CSEE* **2008**, *28* (26), 53−58.
(30) Zhang, S.; Su, Y.; Xiong, Y. Influence of coupling demineralization with the torrefaction pretreatment process on the pyrolysis characteristics and kinetics of rice husk. *Energy Sources, Part A* **2017**, *39* (7), 726−732.
(31) Jiang, L.; Yuan, X.; Li, H.; Xiao, Z.; Liang, J.; Wang, H.; Wu, Z.; Chen, X.; Zeng, G. Pyrolysis and combustion kinetics of sludge-camphor pellet thermal decomposition using thermogravimetric analysis. *Energy Convers. Manage.* **2015**, *106*, 282−289.
(32) Lu, Y.; Wang, Y.; Wang, Q.; Zhang, J.; Zhao, Y.; Zhang, Y. Investigation on the catalytic effect of AAEMs on the pyrolysis characteristics of Changji oil shale and its kinetics. *Fuel* **2020**, *267*, 117287.
(33) Hua, Z.; Wang, Q.; Jia, C.; Liu, Q. Pyrolysis kinetics of a Wangqing oil shale using thermogravimetric analysis. *Energy Sci. Eng.* **2019**, *7* (3), 912−920.
(34) Lin, Y.; Liao, Y.; Yu, Z.; Fang, S.; Lin, Y.; Fan, Y.; Peng, X.; Ma, X. Co-pyrolysis kinetics of sewage sludge and oil shale thermal decomposition using TGA-FTIR analysis. *Energy Convers. Manage.* **2016**, *118*, 345−352.
(35) Maaten, B.; Loo, L.; Konist, A.; Siirde, A. Mineral matter effect on the decomposition of Ca-rich oil shale. *J. Therm. Anal. Calorim.* **2018**, *131*, 2087−2091.
(36) Meng, X.; Qi, Z.; Yu, C.; Bian, J.; Ma, Z.; Long, Q.; Su, J. Solid-Acid Catalytic Conversion of Oil Shale: Effects of Sulfonic Acid Grafting on Oil Yield Enhancing and Quality Improvement. *ACS Omega* **2021**, *6* (8), 5836−5845.
(37) Yan, J.; Jiang, X.; Han, X.; Liu, J. A TG-FTIR investigation to the catalytic effect of mineral matrix in oil shale on the pyrolysis and combustion of kerogen. *Fuel* **2013**, *104*, 307−317.
(38) Tang, Y.; Wu, H.; Yan, Y.; Pan, H.; Zhao, L.; Ma, H.; Hu, Z. Research Progress in the Pyrolysis Technology of Oil Shale. *Liaoning Chem. Ind.* **2022**, *51* (08), 1094−1097.
(39) Xu, F.; Wang, B.; Yang, D.; Hao, J.; Qiao, Y.; Tian, Y. Thermal degradation of typical plastics under high heating rate conditions by TG-FTIR: Pyrolysis behaviors and kinetic analysis. *Energy Convers. Manage.* **2018**, *171*, 1106−1115.
(40) Pan, L.; Dai, F.; Li, G.; Liu, S. A TGA/DTA-MS investigation to the influence of process conditions on the pyrolysis of Jimsar oil shale. *Energy* **2015**, *86*, 749−757.
(41) Qing, W.; Xinmin, W.; Shuo, P. Study on the structure, pyrolysis kinetics, gas release, reaction mechanism, and pathways of Fushun oil shale and kerogen in China. *Fuel Process. Technol.* **2022**, *225*, 107058.
(42) Ling, P.; Xu, J.; Liu, T.; An, X.; Wang, X.; Mostafa, M.; Han, H.; Xu, K.; Jiang, L.; Wang, Y.; et al. Pyrolysis kinetics and reaction mechanisms of coal slime for cleaner energy. *J. Anal. Appl. Pyrolysis* **2022**, *168*, 105718.
(43) Bao, L.; Zhang, T.; Liu, Y.; Dou, Z.; Lü, G.; Wang, X.; Ma, J.; Jiang, X. The Most Probable Mechanism Function and Kinetic Parameters of Gibbsite Dissolution in NaOH. *Chin. J. Chem. Eng.* **2010**, *18* (4), 630−634.
(44) Doyle, C. Estimating isothermal life from thermogravimetric data. *J. Appl. Polym. Sci.* **1962**, *6* (24), 639−642.
(45) Shuping, Z.; Yulong, W.; Mingde, Y.; Chun, L.; Junmao, T. Pyrolysis characteristics and kinetics of the marine microalgae

https://doi.org/10.1021/acsomega.3c04780
ACS Omega 2023, 8, 40396−40406

Dunaliella tertiolecta using thermogravimetric analyzer. *Bioresour. Technol.* **2010**, *101* (1), 359−365.
(46) Chen, C.; Ma, X.; He, Y. Co-pyrolysis characteristics of microalgae Chlorella vulgaris and coal through TGA. *Bioresour. Technol.* **2012**, *117*, 264−273.

https://doi.org/10.1021/acsomega.3c04780
ACS Omega 2023, 8, 40396−40406